


Field-driven transition in the $\text{Ba}_{1-x}\text{K}_x\text{Fe}_2\text{As}_2$ superconductor with splayed columnar defects

Akiyoshi Park, Sunseng Pyon, Kengo Ohara, Nozomu Ito, and Tsuyoshi Tamegai
Department of Applied Physics, The University of Tokyo, Hongo, Bunkyo-ku, Tokyo 113-8656, Japan

Tadashi Kambara and Atsushi Yoshida
Nishina Center, RIKEN, 2-1 Hirosawa, Wako, Saitama 351-0198, Japan

Ataru Ichinose
*Central Research Institute of Electric Power Industry, Electric Power Engineering Research Laboratory,
 2-6-1, Nagasaka, Yokosuka-shi, Kanagawa 240-0196, Japan*

 (Received 22 June 2017; revised manuscript received 5 February 2018; published 23 February 2018)

Through 2.6 GeV U irradiations, we have induced bimodal splayed columnar defects in $\text{Ba}_{1-x}\text{K}_x\text{Fe}_2\text{As}_2$ single crystals with splay angles, $\pm 5^\circ$, $\pm 10^\circ$, $\pm 15^\circ$, and $\pm 20^\circ$. Critical current densities through magnetization measurements were carefully evaluated, where a splay angle of $\pm 5^\circ$ brought about the highest J_c . Magneto-optical images close to T_c indicate highly anisotropic discontinuity lines in the remnant state, and with anisotropy increasing with greater splay angles. Moreover, amongst those with splayed columnar defects, anomalous nonmonotonic field dependences of J_c and S with an extrema at some fraction of the matching field are observed. We discuss that such J_c enhancement arises from a field-driven coupling transition in which intervortex interactions reorganize the vortex structure to be accommodated into columnar defects, thereby increasing pinning at higher fields.

DOI: [10.1103/PhysRevB.97.064516](https://doi.org/10.1103/PhysRevB.97.064516)

I. INTRODUCTION

Motion of flux lines in the mixed state of type-II superconductors has a detrimental consequence of impairing its dissipation-less “zero dc resistivity” state. Retaining stability of flux lines has therefore been a challenge as it is a matter of its high technological interest. As a remedy to such a problem, the notion of localizing flux lines within parallel tracks of columns was originally suggested by portraying the highly localized vortex phase as a Bose glass [1]. Such a remarkable enhancement of pinning was confirmed experimentally through observing remarkable increase in the critical current density (J_c) in cuprate [2] and iron-based superconductors (IBSs) [3–9] after incorporating columnar defects via heavy-ion irradiation.

Later, further enhancement of J_c by dispersing the angles of columnar defects was suggested by Hwa *et al.* [10]. As illustrated in Fig. 1(a), for the case of Bose glass phase in which columnar tracks are parallel, thermal activation may prompt a segment of the flux line to extend to a neighboring defect, allowing the rest of the flux to relocate itself without any expenditure of energy, ultimately leading to hopping. On the other hand, for splayed columnar defects, the variable interdefect distance makes relocation of vortex through thermal activation energetically unfavorable, thereby strongly suppressing vortex motion as shown in Fig. 1(b). Moreover, the splayed columnar defects may promote forced entanglement of vortices, additionally enhancing J_c [10]. Nonetheless, tilting the columnar defects above the lock-in angle is inimical to flux pinning, as pinning is most robust when aligned to the applied field [11]. Such an inherent competition between the adverse effect of vortex-field misalignment and beneficial effect of

splaying columnar defects raises a question: which splay angle optimally enhances the J_c . Current knowledge concerning the optimal splay angle is limited to a seminal report on Au-irradiated $\text{YBa}_2\text{Cu}_3\text{O}_{7-\delta}$ crystals in which a splay angle of $\pm 5^\circ$ yielded the largest J_c amongst $\pm 0^\circ$, $\pm 5^\circ$, $\pm 10^\circ$, and $\pm 15^\circ$ [12]. Similar results were also indicated by Park *et al.* in 1.3 GeV U irradiated $\text{YBa}_2\text{Cu}_3\text{O}_{7-\delta}$ thin films [13], and as well as in 6 GeV irradiated $\text{YBa}_2\text{Cu}_3\text{O}_{7-\delta}$ crystals [14]. Yet, the effects of larger splay angles and the effects of splaying columnar defects amongst other superconducting systems with differing vortex structures remain nebulous. Understanding the role of splayed columnar defects in IBSs cultivates an insight into designing improved pinning landscape for serving the best of our purpose.

Previously, in Ref. [15], we explored the effects of incorporating bimodal splayed columnar defects in IBSs through irradiating optimally doped $\text{Ba}_{1-x}\text{K}_x\text{Fe}_2\text{As}_2$ with 2.6 GeV ^{238}U ions, and provided evidence that a splay angle of $\pm 5^\circ$ yields the largest self-field J_c at 2 K. Through this paper, we confirm the same trend through a different set of samples, and reveal via magneto-optical (MO) imaging, the presence of two components in the in-plane J_c : a component perpendicular to the splay plane ($J_c^{\perp\text{splay}}$) and a parallel component ($J_c^{\parallel\text{splay}}$), in which $J_c^{\parallel\text{splay}} > J_c^{\perp\text{splay}}$ at high temperatures. Despite the large anisotropy revealed close to T_c , we discuss that the anisotropy reduces to unity at low temperatures, thus allowing us to compare the self-field J_c value at 2 K between different samples without having to quantify the individual J_c components. Another key result is that we observe a novel vortex phenomenon that brings about an anomalous secondary magnetization peak

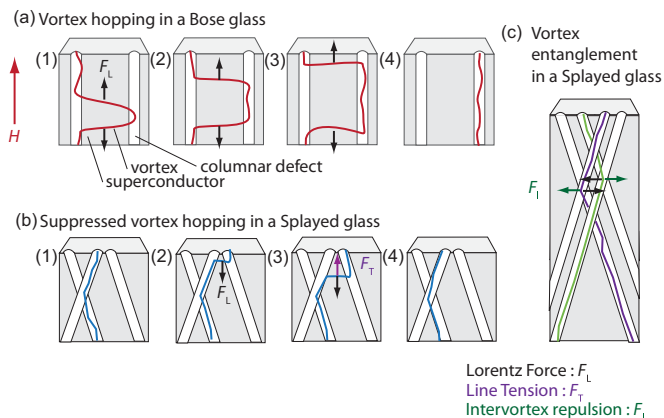


FIG. 1. (a) Model of vortex hopping from one column to another in a Bose glass phase. (b) Reduction of vortex hopping caused by variable interdefect range in a splayed glass phase. (c) Flux entanglement due to intersecting columnar defects in a splayed glass phase.

in the magnetic hysteresis curve when the magnetic field is applied along the average direction of the splayed columnar defects. We provide evidence that such nonmonotonicity is a result of vortex-vortex interactions accommodating flux into columnar defects at higher fields, thereby enhancing pinning.

II. EXPERIMENTAL DETAILS

For this experiment, $\text{Ba}_{1-x}\text{K}_x\text{Fe}_2\text{As}_2$, a prototypical IBS, was employed for investigation. With optimal doping, the T_c reaches 38 K, the highest amongst the BaFe_2As_2 system. Moreover, the small coherence length $\xi_0 = 1.2$ nm [16] in optimally doped $\text{Ba}_{1-x}\text{K}_x\text{Fe}_2\text{As}_2$ compared to optimally doped $\text{BaFe}_2(\text{As}_{1-x}\text{P}_x)_2$ with $\xi_0 = 2.14$ nm [17] and $\text{Ba}(\text{Fe}_{1-x}\text{Co}_x)_2\text{As}_2$ with $\xi_0 = 2.44$ nm [18] indicates that $\text{Ba}_{1-x}\text{K}_x\text{Fe}_2\text{As}_2$ has a substantially higher condensation energy ($\varepsilon_0/4\xi^2$, where ε_0 is the line energy) amongst others, thereby making core pinning prompted by artificial defects to be much more effective. The highest reported enhancement of critical current density in $\text{Ba}_{1-x}\text{K}_x\text{Fe}_2\text{As}_2$ has been achieved through 320 MeV Au and 2.6 GeV U irradiation [19]. Hence, in pursuing a high critical current density through sculpting the most effective pinning landscape, $\text{Ba}_{1-x}\text{K}_x\text{Fe}_2\text{As}_2$ would be an excellent target material.

Here, $\text{Ba}_{1-x}\text{K}_x\text{Fe}_2\text{As}_2$ single crystals were grown through a FeAs flux method. Nominal amounts of Ba : K : FeAs were put with a ratio of $1-x : 1.1x : 4$ into an alumina crucible. For the present case, the optimal doping level $x = 0.40$ was employed. Specifically, Ba plates and K chunks together with FeAs powder were placed inside an alumina crucible in a N_2 atmosphere glove box, then sealed inside a stainless steel tube with a stainless steel cap [20]. The reason why a stainless steel seal was employed is because quartz is understood to react with K, making the quartz brittle upon heating. The assembly was heated up to 1150 °C over a period of 10 h and cooled to 800 °C over a period of 70 h, then finally furnace cooled to room temperature [20]. Within the flux, crystal platelets with dimensions over $1 \times 1 \times 0.05$ mm³ were retrieved. Energy dispersive x-ray (EDX) spectroscopy analysis affirmed homo-

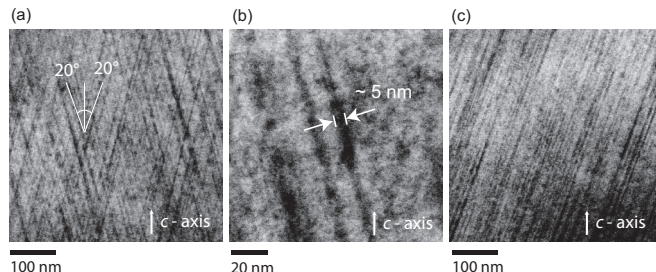


FIG. 2. Transmission electron micrographs of cross-sections of 2.6 GeV U irradiated $\text{Ba}_{1-x}\text{K}_x\text{Fe}_2\text{As}_2$. (a) $\text{Ba}_{1-x}\text{K}_x\text{Fe}_2\text{As}_2$ irradiated with a total dose of 8 T (4 T + 4 T) with a splay angle of $\pm 20^\circ$. Note that the angle shown in the micrographs may appear to be smaller due to slight deviation of the observed cross-sectional plane from the splay plane. (b) A zoomed-in cross-sectional micrograph of the sample in (a) indicating the diameter of the columnar defect. (c) $\text{Ba}_{1-x}\text{K}_x\text{Fe}_2\text{As}_2$ with a total dose of 8 T with tilted columnar defect of angle 20° from the c axis.

geneous doping of $x = 0.40$, and magnetization and resistivity measurements revealed a T_c of 38.6 K. The crystals were cleaved into a rectangular geometry and subject to irradiation.

Uranium irradiation was performed at the RIKEN Nishina Center with ^{238}U ions with energy of 10.75 MeV per nucleon, which translates to 2.6 GeV per ion. The ions were irradiated at room temperature, assuming that annealing of defects do not take place. Moreover, all samples were irradiated with a total matching field of $B_\Phi = 8$ T. Once irradiation was performed, samples were subject to magnetization measurements and MO imaging.

III. RESULTS

A. Defect Structure

For detailed discussions, it is crucial to be aware of the type of defects incorporated in the system. As exhibited in Fig. 2(a), 2.6 GeV U irradiation in $\text{Ba}_{1-x}\text{K}_x\text{Fe}_2\text{As}_2$ indeed introduces linear tracks of columnar defects that cross each other. Opposed to 320 MeV Au irradiation which produces segmented columnar defects [9], 2.6 GeV U irradiation introduces continuous columnar defects, which makes the splay more effective. The diameter of each column is about 3–6 nm [Fig. 2(b)], comparable to the scale of the coherence length. Evidently, the similar case is seen for those irradiated with tilted columnar defects [Fig. 2(c)]. The size makes each of the columns an excellent pinning center for core interaction. Based on the morphology of the defects elucidated through scanning transmission electron microscope observation, the physics of vortex matter will be discussed here on.

B. Anisotropic critical current density

For a bimodal splay system, as in the case here, two components of J_c arise: $J_c^{\parallel\text{splay}}$ and $J_c^{\perp\text{splay}}$, the critical current density that runs in the same direction as the splay plane and critical current density that runs perpendicular to the splay plane. The existence of two different J_c component amongst systems with splayed columnar defects has been confirmed via resistivity measurements in 1 GeV Au irradiated $\text{YBa}_2\text{Cu}_3\text{O}_{7-\delta}$ by Lopez

et al. and in 3.9 GeV Au irradiated YBa₂Cu₃O_{7- δ} by Kwok *et al.*, in which Ohmic dissipation was higher in current running in the direction perpendicular to the splay plane, suggesting that $J_c^{\parallel\text{splay}}$ is larger than $J_c^{\perp\text{splay}}$ [21,22]. Furthermore, the anisotropy in the J_c was found to be pronounced at higher fields, suggestive of the fact that occupation of vortices in the columnar tracks heavily influence the pinning characteristics [21]. In compliment to transport measurements, MO images of DyBa₂Cu₃O_{7- δ} crystals with splayed columnar defects conjointly indicated that $J_c^{\parallel\text{splay}} > J_c^{\perp\text{splay}}$ at high fields with anisotropy increasing at larger fields [23], and inversion in anisotropy where $J_c^{\parallel\text{splay}} < J_c^{\perp\text{splay}}$ at low fields [23].

Yet, no observation has been ever made on IBS systems. Hence, to confirm the existence of an anisotropic J_c in Ba_{1-x}K_xFe₂As₂, the spatial distribution of penetrated flux was observed through MO imaging at the remnant state. Figs. 3(b)–3(d) illustrate the remnant state MO images after sweeping from 1 kOe back to zero field, at a temperature of 1 K below T_c (≈ 37 K) in Ba_{1-x}K_xFe₂As₂ with splayed columnar defects of $\pm 5^\circ$, $\pm 10^\circ$, and $\pm 15^\circ$, respectively. Just below T_c , at 37 K, the flux enters the center of the sample, forming a critical state, thereby leaving a double Y-shaped current discontinuity line.

Unlike the isotropic case, as shown on the pristine crystal [Fig. 3(a)] with a discontinuity line of $\approx 45^\circ$ angle with respect to the sample edge, there is anisotropy in the J_c as evident from the skewed “double Y” discontinuity line, which appears as a consequence of the continuity condition [24,25]. It is noteworthy that even for a small splay angle of $\pm 5^\circ$, a remarkable anisotropy is observed. Consistent to YBa₂Cu₃O_{7- δ} and DyBa₂Cu₃O_{7- δ} with bimodal splayed columnar defects, we can confirm $J_c^{\parallel\text{splay}} > J_c^{\perp\text{splay}}$ for Ba_{1-x}K_xFe₂As₂. Similar trends in the anisotropy were also observed through MO imaging in crystals with $\pm 10^\circ$ and $\pm 15^\circ$ splay angles [Figs. 3(c) and 3(d)]. For further quantitative analysis of the J_c anisotropy, line profiles of the flux density along white (red) dashed lines in Figs. 3(a), 3(b), 3(c), and 3(d) are shown in Figs. 4(a) and 4(b), 4(c) and 4(d), 4(e) and 4(f), and 4(g) and 4(h), respectively. Clearly, the distances of the flux peaks in the discontinuity lines from the sample edge are not equal. Comparing the ratio of the distance of the discontinuity lines from the sample edge along

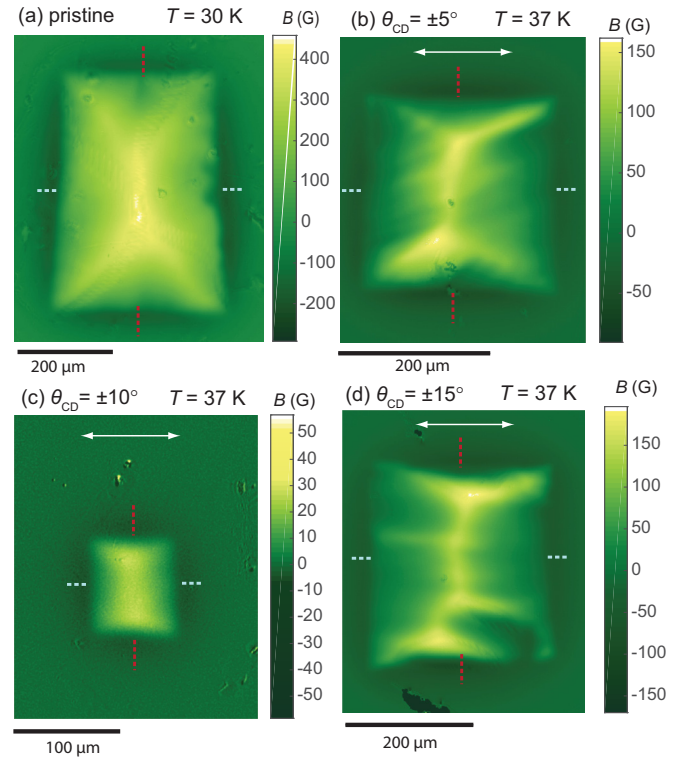


FIG. 3. Magneto-optical images of Ba_{1-x}K_xFe₂As₂ single crystal (a) in the pristine state at $T = 30$ K, and those irradiated with splay angle of (b) $\pm 5^\circ$, (c) $\pm 10^\circ$, and (d) $\pm 15^\circ$ in the remnant state using a field of 1 kOe along the c axis, at $T = 37$ K. The white arrows show the splay direction. Furthermore, the red and white dashed lines depict where the line profiles are extracted.

and perpendicular to the splay, it is clear that the anisotropy increases with increasing splay angle. While the anisotropy of the J_c ($\zeta = J_c^{\parallel\text{splay}} / J_c^{\perp\text{splay}}$) for the pristine crystal is $\zeta = 1$, $\zeta = 1.79$ for $\pm 5^\circ$, $\zeta = 2.63$ for $\pm 10^\circ$, and $\zeta = 4.17$ for $\pm 15^\circ$ splayed columnar defects (Fig. 5). Hence, the J_c in the direction of the splay plane has a value much larger than the J_c in the perpendicular direction.

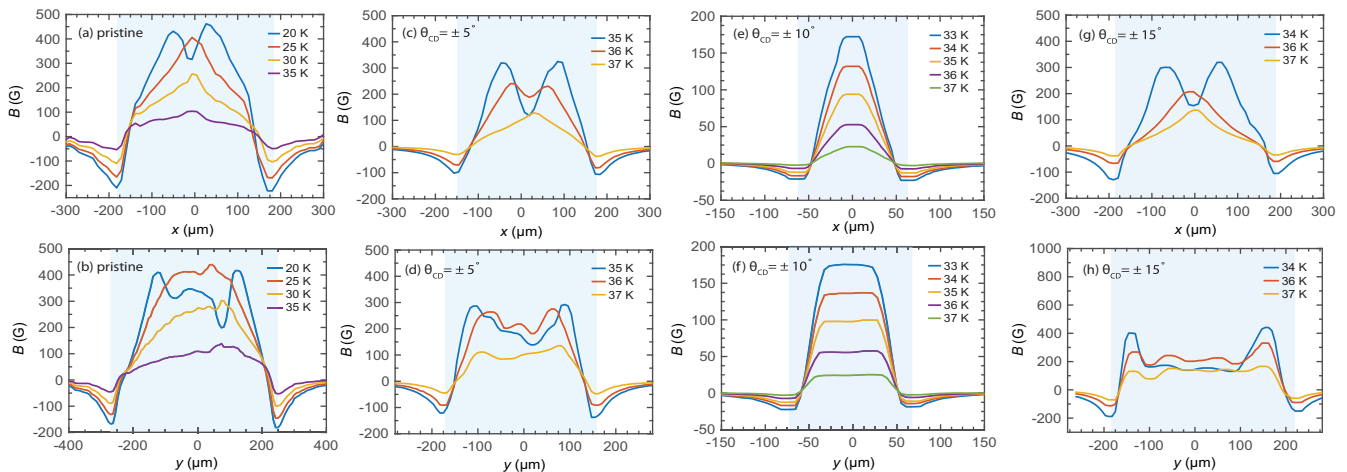


FIG. 4. Line profiles of MO images of Fig. 3 along the white dashed lines (a), (c), (e), (g), and along the red dashed lines (b), (d), (f), (h) at various temperatures. The blue regions indicate the width of the sample.

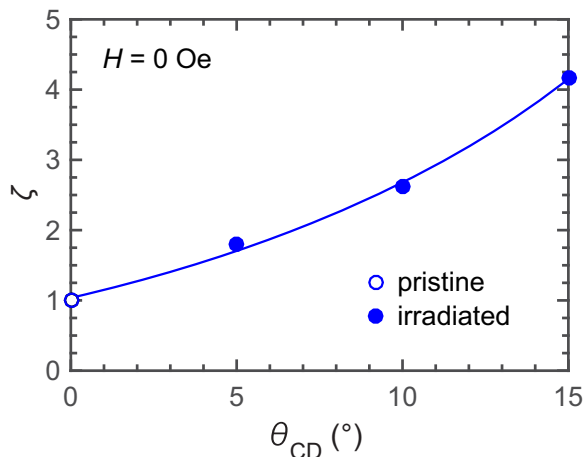


FIG. 5. The splay angle dependence of J_c anisotropy, ζ , calculated from the MO images of Fig. 3, close to T_c in the remnant state.

Schuster *et al.* suggest that the anisotropy in the J_c is due to differences in the activation barrier as a result of a distinct kink nucleation process across and in the same direction of the splay: for $F_L^{\perp\text{splay}}$ ($J_c^{\parallel\text{splay}}$), vortex motion is controlled by zigzag type kinks, whereas for $F_L^{\parallel\text{splay}}$ ($J_c^{\perp\text{splay}}$), vortex motion is manifested by double kinks [21]. López *et al.* further this argument by advocating that the vortex structure is associated with the anisotropic dissipation in the superconductor. The forced entanglement of vortices due to splayed columnar defects is effective only when vortices maintain c -axis coherence. When the c -axis coherence of vortices is lost, vortices lose their identity as a line and are torn apart into decoupled segments of vortices. Such vortex coherence is lost due to thermal decoupling of vortices and in the advent of flux cutting [26,27]. In light of this argument, the anisotropy would be only present at small splay angles since flux cutting is difficult, forcing vortices to entangle. At large splay angles, flux cutting could be achieved easily and flux entanglement would not occur. From MO images obtained in this experiment, even in the low-field regime close to the self-field, the significant J_c anisotropy indicates great degree of flux entanglement. Even at large splay angle of $\pm 15^\circ$, flux entanglement is observed. In stark contrast to such a high degree of anisotropy detected in IBSs at low fields, J_c anisotropy is almost nullified in the remnant state magnetization among $\text{YBa}_2\text{Cu}_3\text{O}_{7-\delta}$ and $\text{DyBa}_2\text{Cu}_3\text{O}_{7-\delta}$ single crystals [21,23]. This implicitly suggests that vortex coherence in IBSs are more robust than that of cuprates, as there is smaller anisotropy in coherence length amongst IBSs.

C. Global critical current density

The relationship between the anisotropic critical current density and the magnetization for when $J_c^{\parallel\text{splay}}/J_c^{\perp\text{splay}} > a/b$, where a and b are the dimensions of the crystal, is given by

$$\Delta M = \frac{J_c^{\perp\text{splay}} a}{20} \left(1 - \frac{a}{3b} \frac{J_c^{\perp\text{splay}}}{J_c^{\parallel\text{splay}}} \right) \quad (1)$$

[24]. Although the two components of J_c were decomposed through MO imaging at temperatures close to T_c at the remnant state, determining the value of the individual J_c components

at higher fields cannot be performed by this method due to saturation of the Faraday rotation of the garnet indicator film. Another method is through transport measurements. Yet, this method would require applying a large current on the sample, or alternatively preparing a thin sample, which are both technically difficult. Hence, we build our discussion based on global magnetization measurements, and calculate the overall J_c given by the isotropic Bean's model, and compare the values between different splay angles, as done in Ref. [12].

In the conventional method, the width of the hysteresis loop ΔM , which is the difference between M sweeping downfield, and then back upfield is used. However, since the self-field is significant, the return branch will cause a non-negligible effect on the calculation of J_c . Hence, instead, the reversible linear background was first obtained through calculating the average of the magnetization of the second and the third quadrant. This linear background component was subtracted from the raw data so that the hysteresis is virtually an even function, $M(H) = M(-H)$. This allows for the calculation of the J_c from the magnetization of the second quadrant of the magnetic hysteresis using the extended isotropic Bean model,

$$J_c = \frac{40M}{a(1 - a/3b)}. \quad (2)$$

The error of J_c due to the deviation of $M(H)$ from an ideal even function is estimated to be less than 8%.

Figure 6 displays the $J_c(H)$ calculated from magnetic hysteresis loops. As indicated in Fig. 6(a), the self-field J_c of pristine crystals at 2 K exhibits a value of 2.6 MA/cm², consistent with other reports [19,28], while irradiated samples reveal a J_c over 10 MA/cm², signifying substantial increase in flux pinning with incorporation of columnar defects. We see that for the case of parallel defects, there is a significant increase in the J_c , exhibiting a typical monotonic decrease with increasing field.

Figures 6(c)–6(f) indicate the J_c as a function of magnetic field at various splay angles ranging from $\pm 5^\circ$ to $\pm 20^\circ$. To compare the effects of the splayed columnar defects, we compare the value of J_c at 2 K under self-field. Given that the samples are approximate squares (i.e., $a \approx b$), the two components differ from the overall J_c by a factor

$$J_c^{\perp\text{splay}} = \frac{2}{3 - 1/\zeta} J_c, \quad (3)$$

$$J_c^{\parallel\text{splay}} = \frac{2\zeta}{3 - 1/\zeta} J_c. \quad (4)$$

As shown in $\text{YBa}_2\text{Cu}_3\text{O}_{7-\delta}$ and $\text{DyBa}_2\text{Cu}_3\text{O}_{7-\delta}$ single crystals, the anisotropy ζ in a system with bimodal splayed columnar defects has an intricate dependence on the field and temperature [21,23]. In this paper, to circumvent such complexities, we strictly limit our discussion on the average critical current density, J_c , obtained through magnetization measurements.

At 2 K under self-field, for the case of those irradiated with parallel columnar defects [Fig. 6(b)], the J_c exhibits a value of 13.9 MA/cm². The value of J_c obtained in this paper for parallel columnar defects is comparable to that in the previous report of J_c in 2.6 GeV U irradiated optimal $\text{Ba}_{1-x}\text{K}_x\text{Fe}_2\text{As}_2$ [19]. Strikingly, the J_c of samples irradiated with a splay angle

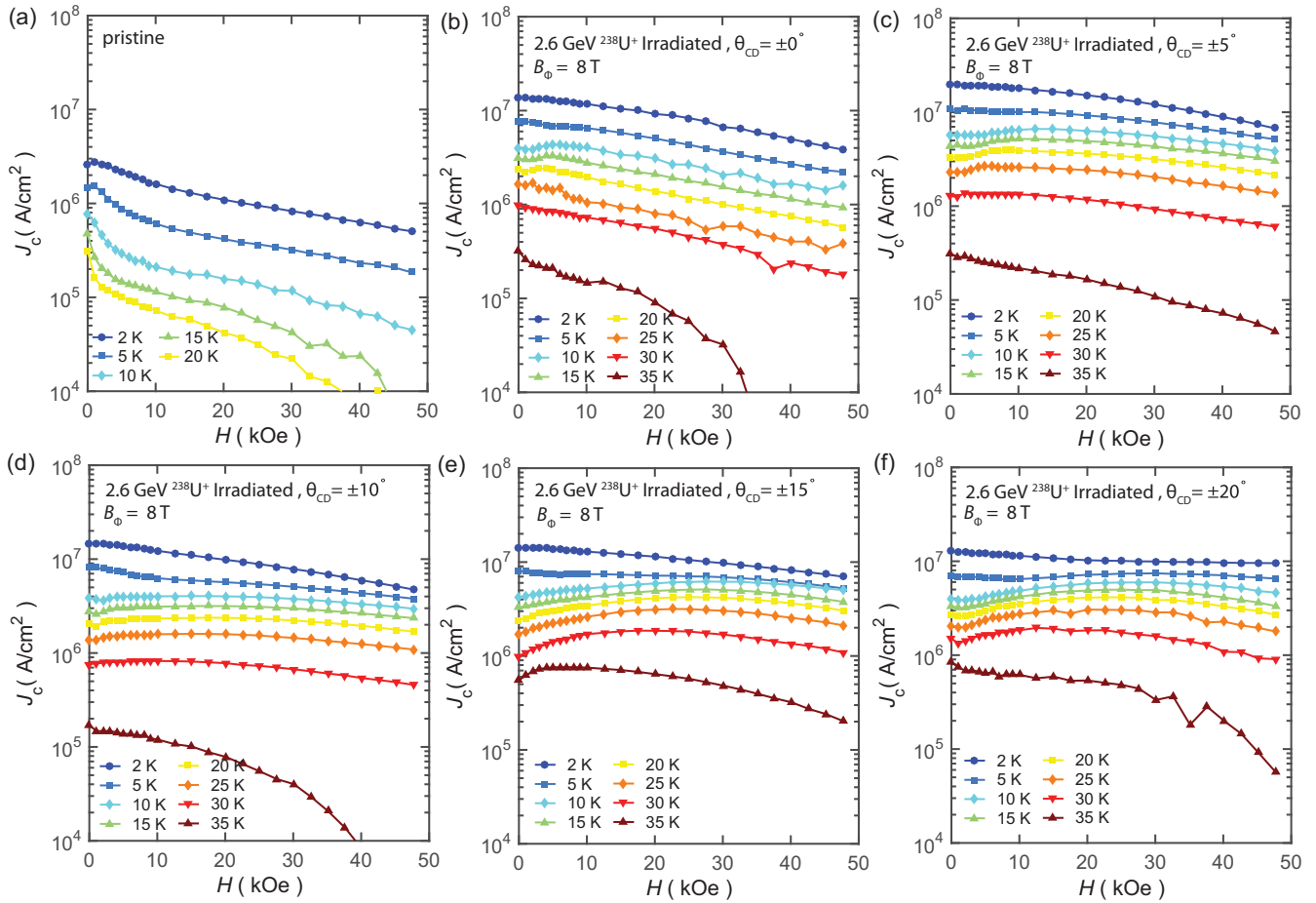


FIG. 6. Magnetic field dependence of J_c in Ba_{1-x}K_xFe₂As₂ of (a) pristine sample and those after ²³⁸U irradiation with (b) parallel defects and splay angle of (c) $\pm 5^\circ$, (d) $\pm 10^\circ$, (e) $\pm 15^\circ$, and (f) $\pm 20^\circ$.

of $\pm 5^\circ$ at 2 K displays a value of 19.5 MA/cm², exceeding those with parallel columnar defects and larger splay angles under all field ranges (Fig. 7). Moreover, it is clear that splay angles larger than $\pm 5^\circ$ exhibit a lower J_c , suggesting that the effects of vortex-field misalignment outperforms the enhancement effect of splayed defects when the tilt angle

of columnar defects increases. This result is consistent with YBa₂Cu₃O_{7- δ} single crystals in Ref. [12], where $\pm 5^\circ$ was reported to be the optimal splay angle with decreasing J_c at higher splay angles.

Not to mention, amongst those with splayed columnar defects, there is an apparent nonmonotonicity in the J_c with increasing field (Fig. 6). Intuitively, the J_c should monotonically decrease with increasing fields due to larger driving force to pull the vortex from its pinning center. For the case of the pristine sample, the highest J_c at all temperature regimes reside at remnant magnetization. Upon inducing parallel columnar defects, a peaklike behavior appears at intermediate temperatures and at low fields. Such behavior can be inferred to originate from the curvature of vortices around the self-field, which induces depinning [9]. However, in those with splayed columnar defects, a much larger and broader peak occurs at higher fields. Since the self-field effects do not occur at large fields, the nonmonotonic behavior arising in a system with splayed columnar defects differs from that with parallel defects.

D. Effects of Tilted Fields

To further investigate the effects of vortex entanglement in the magnetization amongst systems with splayed columnar defects, the magnetization was measured while tilting the angle

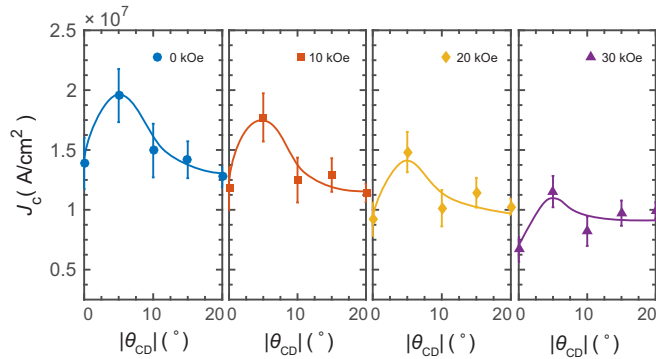


FIG. 7. Splay angle dependence of J_c in Ba_{1-x}K_xFe₂As₂ at 2 K under various applied fields. Evidently, the highest J_c is achieved at small splay angles. The error bars indicate the possible error in J_c , stemming from the error in the measurement of crystal thickness c with uncertainty of 1.5 μ m.

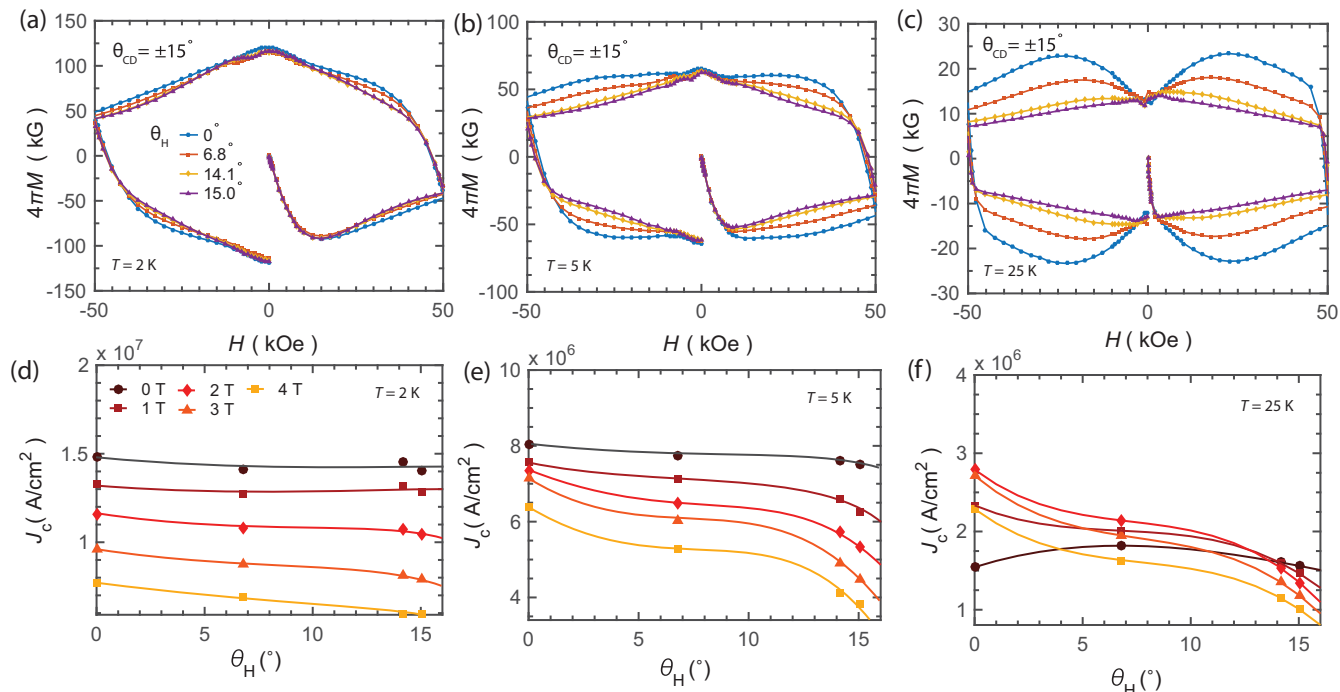


FIG. 8. Magnetic hysteresis loops of $\text{Ba}_{1-x}\text{K}_x\text{Fe}_2\text{As}_2$ with bimodal splay columnar defects of $\theta_{CD} = \pm 15^\circ$ with a total dose of $B_\Phi = 8$ T in tilted fields of various angles at (a) 2 K, (b) 5 K, and (c) 25 K. The J_c dependence of the angle of tilted field at (d) 2 K, (e) 5 K, and (f) 25 K.

of the field in the direction of the splay plane (Fig. 8). Since the magnetization is detected only in the direction of the field, the actual magnetization of the sample is compensated by multiplying by a factor of $1/\cos(\theta_H)$. At the lowest temper-

ature, the magnetization is independent of the angle of the tilted field as indicated by the flat field-angle (θ_H) dependence exhibited in Fig. 8(d). The effect of tilted field becomes more prominent at higher temperatures, where vortices are less rigid.

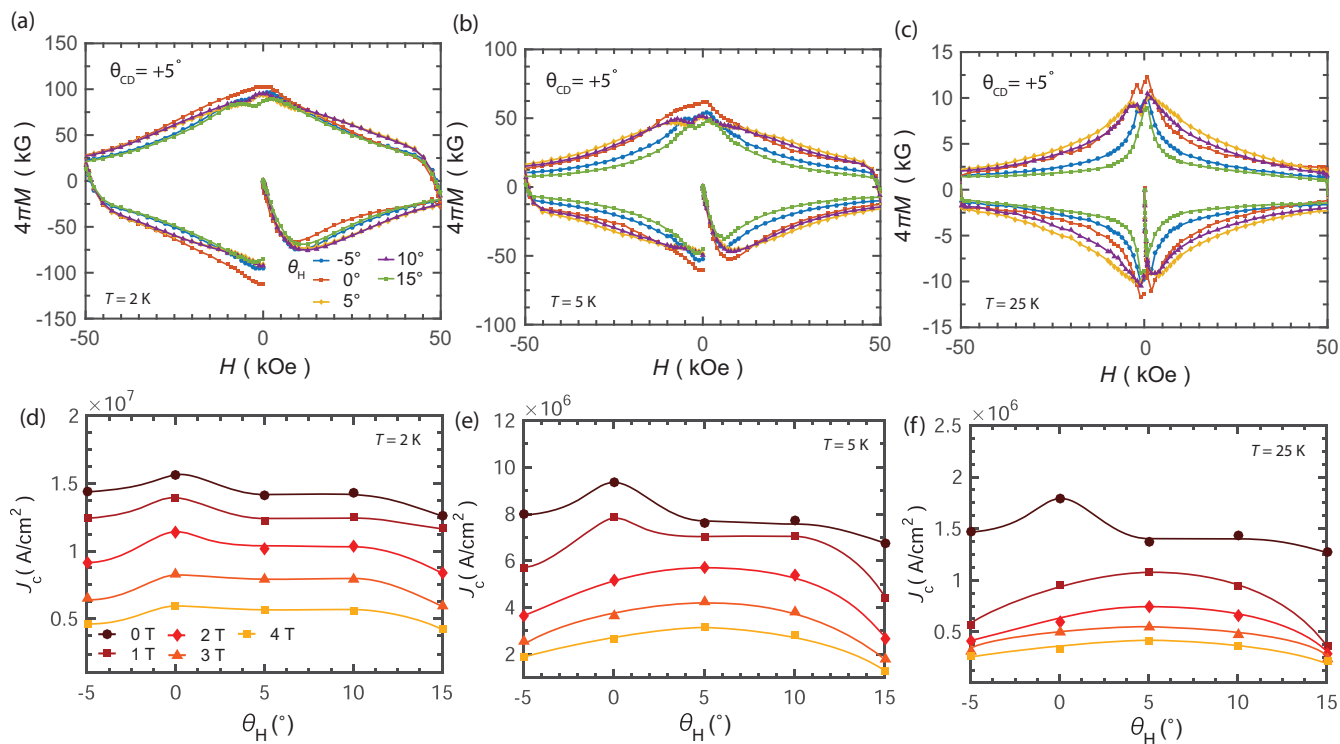


FIG. 9. Magnetic hysteresis loops of $\text{Ba}_{1-x}\text{K}_x\text{Fe}_2\text{As}_2$ with tilted columnar defects of $\theta_{CD} = 5^\circ$ with a total dose of $B_\Phi = 8$ T in tilted fields of various angles at (a) 2 K, (b) 5 K, and (c) 25 K. The tilt-angle dependence of J_c at (d) 2 K, (e) 5 K, and (f) 25 K.

By tilting the field closer to one of the two modes of columnar defects, surprisingly, the nonmonotonic behavior is completely eradicated, with a hysteresis reminiscent of that observed in crystals with parallel columnar defects as shown in Fig. 6(b). Remarkably, the J_c is significantly higher in the case when $\theta_H \parallel c$ than $\theta_H = \theta_{CD}$ at high fields, similar to the behavior of the J_c angular dependence of 270 MeV Xe irradiated $\text{REBa}_2\text{Cu}_3\text{O}_y$ coated conductors [29,30].

We compare this to the case with a tilted (single-mode) columnar defect system of $\theta_{CD} = 5^\circ$. As shown in Fig. 9, the nonmonotonic behavior seen in splayed systems is absent. Hence, clearly the nonmonotonicity in the field dependence of J_c is characteristic to systems with splayed columnar defects. Although the J_c is almost independent of θ_H at low temperatures, the differences become more prominent at higher temperatures. At high fields (2 T or larger), where self-field effect does not play a role, the highest J_c occurs when $\theta_H = \theta_{CD}$. This is due to the energetically stable flux composition in which it is aligned to the external magnetic field.

E. Magnetic Relaxation Rate

Amongst $\text{YBa}_2\text{Cu}_3\text{O}_{7-\delta}$ single crystal, one intriguing feature is, while splay enhances the critical current density, especially in those with small splay angles, flux creep is reported to be promoted upon incorporation of splayed columnar defects [12,31]. Figure 10 illustrates the field dependence of the

normalized magnetic relaxation rate S defined by

$$S = \left| \frac{d \ln(M)}{d \ln(t)} \right|, \quad (5)$$

for splay angles of $\pm 5^\circ$ and $\pm 15^\circ$ at 25 K. Clearly, the field dependence of S in splayed systems are distinct from those with parallel columnar defects (2.6 GeV U ions with a dose of 8 T) [19]. It is noteworthy that at higher fields, relaxation rate in sample with $\theta_{CD} = \pm 5^\circ$ is higher than that with $\theta_{CD} = \pm 15^\circ$. Most importantly, the field dependence of the critical current densities are depicted to be mirror images of the field dependence of the relaxation rate. The local maxima in the J_c for $\pm 15^\circ$ corresponds to the local minima in S . Such mirror-image correspondence between S and J_c has been observed in both cuprates and IBSs [32,33].

IV. DISCUSSIONS

Up to this point, we have observed an anomalous behavior in vortex pinning and vortex dynamics in those with splayed columnar defects at intermediate temperatures. Moreover, remarkably, when tilting the field along the splay plane, the anomalous peak in the magnetization is eliminated. To reveal such strange behavior, we expand our discussion on the vortex structure amongst systems with splayed columnar defects in IBSs.

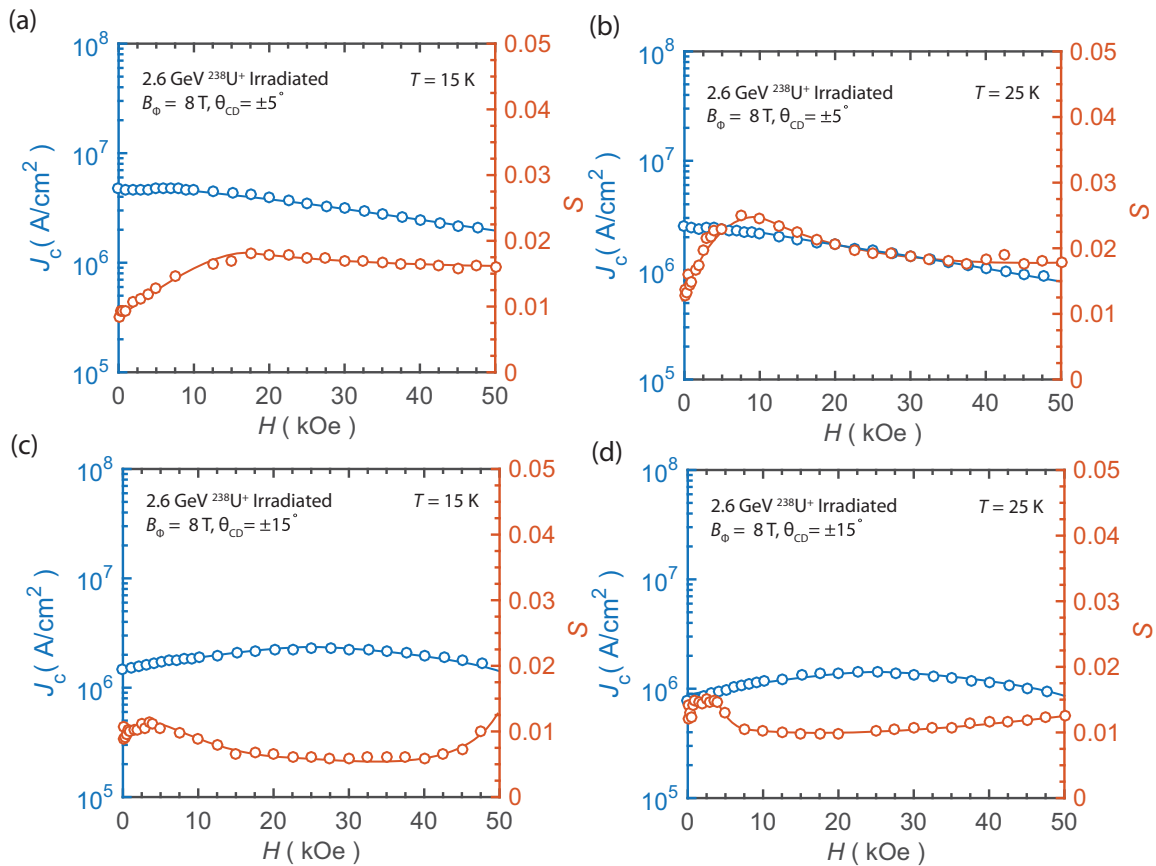


FIG. 10. The field dependence of the normalized relaxation rate of $\text{Ba}_{1-x}\text{K}_x\text{Fe}_2\text{As}_2$ with splay of $\pm 5^\circ$ at (a) 15 K and (b) 25 K. Similarly, S for splay of $\pm 15^\circ$ at (c) 15 K and (d) 25 K.

We begin by considering the angular behavior of the pinning energy per unit length (U'_p) in a system with columnar defects [34,35],

$$U'_p \approx \varepsilon_0 \left(\frac{2k_B T \tan(\theta_{\text{acc}})}{\varepsilon_0 a_0} \right)^{2/3}, \quad (6)$$

where $\varepsilon_0 = (\Phi_0/4\pi\lambda_{ab})^2$ is the vortex line energy, $a_0 = \sqrt{\Phi_0/B}$ is the average intervortex spacing, and θ_{acc} is the accommodation angle. The vortex accommodation angle is obtained from the vortex lock-in angle using the following relationship:

$$\theta_L = \frac{4\pi\varepsilon_l}{\Phi_0 B} \theta_{\text{acc}} \quad (7)$$

[1,36,37], in which $\varepsilon_l = \varepsilon_0 \ln(\kappa)$ is the line tension, with $\kappa = \lambda/\xi$ being the Ginzburg-Landau parameter. For this case, we use the experimentally obtained lock-in angle (θ_L) reported in Ref. [38]. We note that, although the lock-in angle obtained in Ref. [38] is that of 2.6 GeV U irradiated Ba(Co_{1-x}Fe_x)₂As₂, since Ba_{1-x}K_xFe₂As₂ has similar anisotropy, we estimate that the lock-in angle should be no different for both cases. Thus, using $\xi(0) = 1.2$ nm [16], and $\lambda(0) = 200$ nm [39], along with the temperature dependences $\xi(T) = \xi(0)(1 - T/T_c)^{-1/2}$, $\lambda(T) = \lambda(0)(1 - T/T_c)^{-1/2}$, we obtain $\xi(25\text{ K}) = 2.1$ nm and $\lambda(25\text{ K}) = 340$ nm, allowing us to acquire a value of $\theta_{\text{acc}} = 41.4^\circ$, which is field-independent.

We compare this value to the actual pinning energy in the system with splayed columnar defects U_p by considering the inverse power-law barrier proposed by Feigel'man:

$$U = U_p \left(\left(\frac{J_{c0}}{J} \right)^\mu - 1 \right) \quad (8)$$

[40]. Here, U is the effective activation energy, J is the current density, J_{c0} is the critical current density required to nullify the activation energy, and μ is the glassy exponent. The value of U_p is obtained using Eq. (8) to fit the experimentally obtained magnetic relaxation data scaled by Maley's relationship,

$$U = -k_B T \left(\ln \left(\frac{dM}{dt} \right) - C \right), \quad (9)$$

through a nonlinear least-squares method, where C in Eq. (9) is an arbitrary constant, which we fix with the value $C = 30$ for samples with splay angles of $\pm 5^\circ$ and $\pm 15^\circ$, and $C = 20$ for sample with parallel columnar defects [41]. Upon fitting, we consider the temperature dependence $U_p = U_{p0}(1 - (T/T_c)^2)^{3/2}$ [42], and fix the glassy exponent $\mu = 7/9$ at the large vortex bundle regime (i.e., Larkin lengths are larger than the penetration depth) since the vortices are expected to be highly correlated with such a high degree of disorder. Thus we obtain the field dependence of the activation barrier as exhibited in Fig. 11(a).

From U_p and U'_p , we can obtain the effective length of the vortex segment trapped in the columnar defect (l_p):

$$l_p \approx U_p / U'_p \quad (10)$$

[22]. Figure 11(b) illustrates the evolution of l_p with increasing field at a temperature of 25 K. It becomes evident that for the case when columnar defects are parallel ($\theta_{\text{CD}} = \pm 0^\circ$), l_p decreases with increasing field and becomes field independent

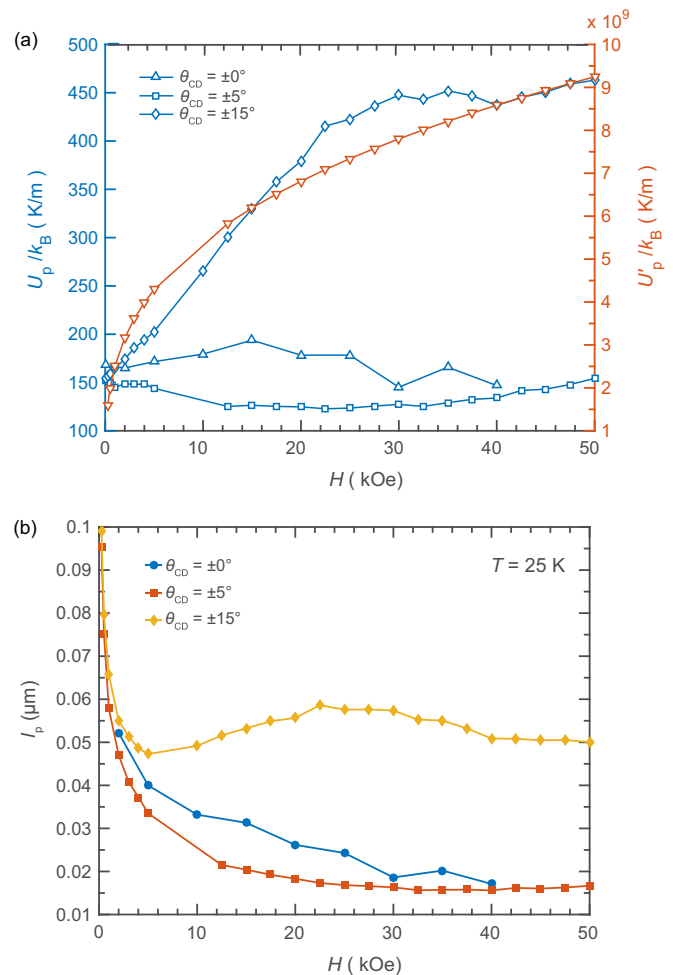


FIG. 11. (a) The field dependence of U_p and U'_p at 25 K for samples with splayed columnar defects with angles $\pm 0^\circ$, $\pm 5^\circ$, and $\pm 15^\circ$. (b) The field dependence of l_p calculated from U_p and U'_p .

at a value of $l_p \approx 0.02 \mu\text{m}$. Similarly, for the case of $\theta_{\text{CD}} = \pm 5^\circ$, there is a steady decrease in l_p upon an increase in the field, reaching a value of $\approx 0.02 \mu\text{m}$ at a field of 50 kOe. Even more strikingly, for $\theta_{\text{CD}} = \pm 15^\circ$, a less rapid decrease in l_p is evident, where $l_p \approx 0.05 \mu\text{m}$ at a field of 50 kOe. Hence, amongst a splayed glass phase, there is an apparent robustness in the effective length of the vortex segment pinned to the columnar defect with an increase in field.

From such observation, we infer that the vortex structure with parallel columnar defects at low fields are essentially linear with a certain number of kinks that reach out to neighboring columns due to thermal fluctuations as illustrated in Fig. 12(a). As the field increases, the overall vortex density increases with significant intervortex interaction. Yet, the passive change in l_p value entails that the vortex structure remains largely unaltered [Fig. 12(b)].

For the case with splayed columnar defects at low fields, the vortices are fundamentally trapped in the columnar defects with some thermally activated kinks as depicted in Fig. 12(c). Upon increasing the field, the vortices are accommodated into the defects, forming a “zigzag” configuration, as reflected in the increase in l_p . Since a higher degree of pinned vortex length

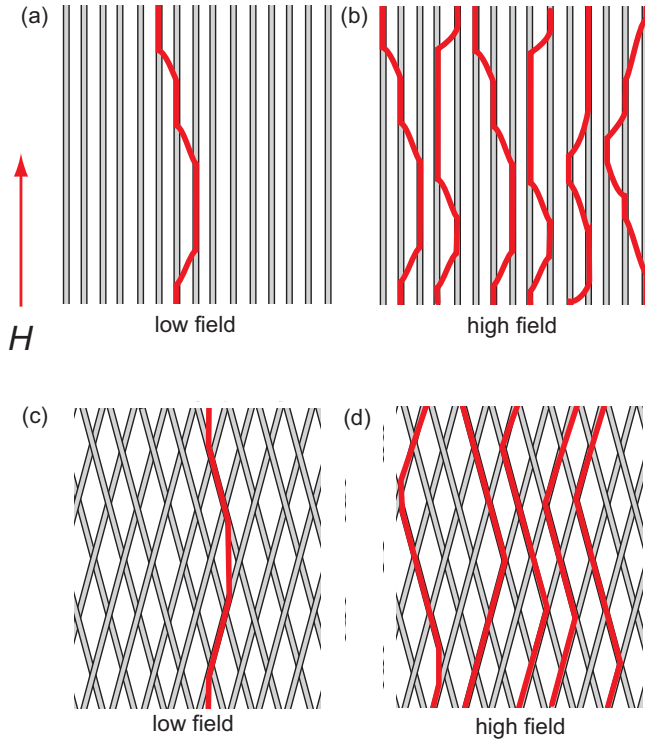


FIG. 12. Schematics of the vortex structure in a Bose glass phase at (a) low fields and at (b) high fields at a temperature of 25 K. The vortex structure in a splayed glass phase (c) at low fields and (d) at high fields.

results in a stronger pinning, we suggest that such change in the vortex structure could be highly related to the nonmonotonic field dependence of J_c .

In regard to this framework, we must explicate why the nonmonotonic field dependence is eliminated when the field is applied in the direction that corresponds to one of the modes of the bimodal splay. As shown in Fig. 13(a), since one of the modes of the splay is already in line with the field, it is anticipated that the vortex should be linear, as it is the most energetically stable configuration. Therefore, even in high-field regimes, the vortex configuration remains

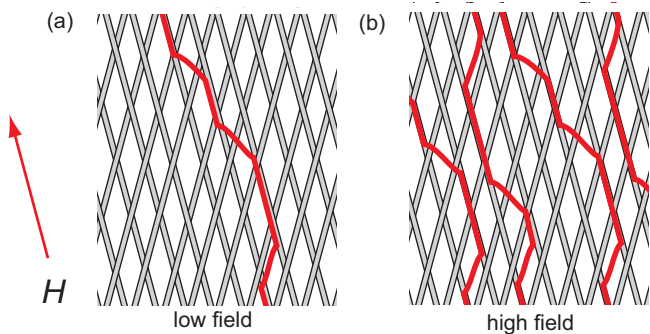


FIG. 13. Schematics of the vortex structure in a splayed glass phase (a) at low fields and (b) at high fields when the field is applied in the direction that corresponds to one of the modes of the columnar defects.

unchanged [Fig. 12(b)], as with the case of parallel columnar defects, thereby resulting in a conventional monotonic field dependence of J_c .

A similar phenomenon of J_c enhancement has been reported to occur in heavy-ion irradiated $\text{YBa}_2\text{Cu}_3\text{O}_{7-\delta}$ single crystals [2,43]. Such a phenomenon arises at a field of $1/5 \sim 1/3 B_\Phi$, which corresponds to the field range of the peak seen in this case. Although the reported $\text{YBa}_2\text{Cu}_3\text{O}_{7-\delta}$ crystals were irradiated parallel to the c axis by heavy ions, cross-sectional TEM images reveal naturally induced splayed columnar defects [2]. Moreover, consistent to U-irradiated IBSs in this investigation, only when the field is in the same direction of the c axis, the nonmonotonic behavior ensues, while disappearing when tilted in an angle. To explicate this behavior, it has been suggested that the nonmonotonicity of J_c emanates from increased intervortex repulsion, which increases the vortex trapping rate by columnar defects. As a result of amplified vortex trapping, increased interlayer coupling coherence of vortices is achieved. Indeed, enhancement of interlayer coherence has been confirmed experimentally through Josephson plasma resonance measurements in heavy-ion irradiated $\text{Bi}_2\text{Sr}_2\text{CaCu}_2\text{O}_{8+y}$, signifying the enhancement of vortex trapping. The similarities between the two systems with splayed columnar defects suggests that the nonmonotonic field dependence of J_c in this framework is possibly a universal behavior that does not only apply to IBSs.

V. CONCLUSION

Through this paper, we have initially revealed four main observations. (1) By introducing a bimodal splay through U-irradiation, $\text{Ba}_{1-x}\text{K}_x\text{Fe}_2\text{As}_2$ single crystals exhibit a highly anisotropic J_c with even greater anisotropy with larger splay angles. (2) A system with a splay angle of $\pm 5^\circ$ reveals an optimal J_c with a high value of 19.5 MA/cm^2 . (3) Third, and most importantly, amongst a splayed glass phase, an anomalous nonmonotonic field dependence of J_c and S arises. (4) Last but not least, through tilting the field so that the field is aligned to one of the two modes of splay, the nonmonotonic J_c dependence is strangely eradicated.

To interpret such salient nonmonotonicity in the field dependence of J_c , we examine the evolution of the effective length of a vortex segment trapped in the columnar defect l_p with increasing magnetic field, and reveal that systems with splayed columnar defects exhibit a larger value in l_p than that in those with parallel columnar defects. The accommodation of vortices into columnar defects in splayed systems are reminiscent of the field-driven interlayer recoupling transition behavior seen in heavy-ion irradiated cuprates. Such reported phenomena and the one seen in this investigation are highly consistent, as they appear in similar field ranges. However, there is an essential difference between the two such that, while in cuprates, the J_c nonmonotonicity is seen in those with parallel columnar defects, we see that the behavior is absent amongst IBSs with parallel columnar defects and only present in those with splayed columnar defects. We discuss that the inherent disparity is due to differences in the strength of the vortex interlayer coupling and the defect morphology apparent in the two systems.

Finally, we reiterate the fact that the investigation presented here is based on analysis of the average in-plane J_c rather than treating the individual J_c components. Further analysis on the effects on the anisotropy of J_c induced by splayed columnar defects would further shed light into the complex vortex behavior in such systems.

ACKNOWLEDGMENTS

This experiment was performed at RI Beam Factory operated by RIKEN Nishina Center and CNS, The University of Tokyo. This paper is partly supported by KAKENHI (17H01141) from JSPS.

-
- [1] D. R. Nelson and V. M. Vinokur, *Phys. Rev. B* **48**, 13060 (1993).
- [2] L. Civale, A. D. Marwick, T. K. Worthington, M. A. Kirk, J. R. Thompson, L. Krusin-Elbaum, Y. Sun, J. R. Clem, and F. Holtzberg, *Phys. Rev. Lett.* **67**, 648 (1991).
- [3] Y. Nakajima, Y. Tsuchiya, T. Taen, T. Tamegai, S. Okayasu, and M. Sasase, *Phys. Rev. B* **80**, 012510 (2009).
- [4] R. Prozorov, M. A. Tanatar, B. Roy, N. Ni, S. L. Bud'ko, P. C. Canfield, J. Hua, U. Welp, and W. K. Kwok, *Phys. Rev. B* **81**, 094509 (2010).
- [5] L. Fang, Y. Jia, C. Chaparro, G. Sheet, H. Claus, M. A. Kirk, A. E. Koshelev, U. Welp, G. W. Crabtree, W. K. Kwok, S. Zhu, H. F. Hu, J. M. Zuo, H.-H. Wen, and B. Shen, *Appl. Phys. Lett.* **101**, 012601 (2012).
- [6] L. Fang, Y. Jia, V. Mishra, C. Chaparro, V. K. Vlasko-Vlasov, A. E. Koshelev, U. Welp, G. W. Crabtree, S. Zhu, N. D. Zhigadlo, S. Katrych, J. Karpinski, and W. K. Kwok, *Nat. Commun.* **4**, 2655 (2013).
- [7] K. J. Kihlstrom, L. Fang, Y. Jia, B. Shen, A. E. Koshelev, U. Welp, G. W. Crabtree, W.-K. Kwok, A. Kayani, S. F. Zhu, and H.-H. Wen, *Appl. Phys. Lett.* **103**, 202601 (2013).
- [8] N. Haberkorn, J. Kim, K. Gofryk, F. Ronning, A. S. Sefat, L. Fang, U. Welp, W. K. Kwok, and L. Civale, *Supercond. Sci. Technol.* **28**, 055011 (2015).
- [9] T. Tamegai, T. Taen, H. Yagyuda, Y. Tsuchiya, S. Mohan, T. Taniguchi, Y. Nakajima, S. Okayasu, M. Sasase, H. Kitamura, T. Murakami, T. Kambara, and Y. Kanai, *Supercond. Sci. Technol.* **25**, 084008 (2012).
- [10] T. Hwa, P. Le Doussal, D. R. Nelson, and V. M. Vinokur, *Phys. Rev. Lett.* **71**, 3545 (1993).
- [11] L. Civale, L. Krusin-Elbaum, J. R. Thompson, R. Wheeler, A. D. Marwick, M. A. Kirk, Y. R. Sun, F. Holtzberg, and C. Feild, *Phys. Rev. B* **50**, 4102 (1994).
- [12] L. Krusin-Elbaum, A. D. Marwick, R. Wheeler, C. Feild, V. M. Vinokur, G. K. Leaf, and M. Palumbo, *Phys. Rev. Lett.* **76**, 2563 (1996).
- [13] J. H. Park, D. Kim, S. Shim, Y. Kim, J. Lee, T. Hahn, J. Hettlinger, D. Steel, K. Gray, B. Glagola, J. Lee, and Z. Khim, *Physica C* **281**, 310 (1997).
- [14] V. Hardy, S. Hébert, C. Goupil, C. Simon, J. Provost, M. Hervieu, and P. Lejay, *Phys. Rev. B* **59**, 8455 (1999).
- [15] A. Park, S. Pyon, T. Tamegai, and T. Kambara, *Physica C* **530**, 58 (2016), 28th International Symposium on Superconductivity.
- [16] U. Welp, R. Xie, A. E. Koshelev, W. K. Kwok, H. Q. Luo, Z. S. Wang, G. Mu, and H. H. Wen, *Phys. Rev. B* **79**, 094505 (2009).
- [17] C. Chaparro, L. Fang, H. Claus, A. Rydh, G. W. Crabtree, V. Stanev, W. K. Kwok, and U. Welp, *Phys. Rev. B* **85**, 184525 (2012).
- [18] A. Yamamoto, J. Jaroszynski, C. Tarantini, L. Balicas, J. Jiang, A. Gurevich, D. C. Larbalestier, R. Jin, A. S. Sefat, M. A. McGuire, B. C. Sales, D. K. Christen, and D. Mandrus, *Appl. Phys. Lett.* **94**, 062511 (2009).
- [19] F. Ohtake, T. Taen, S. Pyon, T. Tamegai, S. Okayasu, T. Kambara, and H. Kitamura, *Physica C* **518**, 47 (2015).
- [20] K. Kihou, T. Saito, S. Ishida, M. Nakajima, Y. Tomioka, H. Fukazawa, Y. Kohori, T. Ito, S. ichi Uchida, A. Iyo, C.-H. Lee, and H. Eisaki, *J. Phys. Soc. Jpn.* **79**, 124713 (2010).
- [21] D. López, L. Krusin-Elbaum, H. Safar, V. M. Vinokur, A. D. Marwick, J. Z. Sun, and C. Feild, *Phys. Rev. Lett.* **79**, 4258 (1997).
- [22] W. K. Kwok, L. M. Paulius, V. M. Vinokur, A. M. Petrean, R. M. Ronningen, and G. W. Crabtree, *Phys. Rev. B* **58**, 14594 (1998).
- [23] T. Schuster, H. Kuhn, M. Indenbom, M. Leghissa, M. Kraus, and M. Konczykowski, *Phys. Rev. B* **51**, 16358 (1995).
- [24] E. M. Gyorgy, R. B. van Dover, K. A. Jackson, L. F. Schneemeyer, and J. V. Waszczak, *Appl. Phys. Lett.* **55**, 283 (1989).
- [25] T. Schuster, H. Kuhn, M. V. Indenbom, G. Kreiselmeyer, M. Leghissa, and S. Klaumünzer, *Phys. Rev. B* **53**, 2257 (1996).
- [26] A. Sudbø and E. H. Brandt, *Phys. Rev. Lett.* **67**, 3176 (1991).
- [27] M. A. Moore and N. K. Wilkin, *Phys. Rev. B* **50**, 10294 (1994).
- [28] T. Taen, F. Ohtake, S. Pyon, T. Tamegai, and H. Kitamura, *Supercond. Sci. Technol.* **28**, 085003 (2015).
- [29] T. Sueyoshi, Y. Furuki, T. Kai, T. Fujiyoshi, and N. Ishikawa, *Physica C* **504**, 53 (2014).
- [30] T. Sueyoshi, T. Nishimura, T. Fujiyoshi, F. Mitsugi, T. Ikegami, and N. Ishikawa, *Supercond. Sci. Technol.* **29**, 105006 (2016).
- [31] J. R. Thompson, L. Krusin-Elbaum, L. Civale, G. Blatter, and C. Feild, *Phys. Rev. Lett.* **78**, 3181 (1997).
- [32] L. Krusin-Elbaum, L. Civale, V. M. Vinokur, and F. Holtzberg, *Phys. Rev. Lett.* **69**, 2280 (1992).
- [33] N. Ni, M. E. Tillman, J.-Q. Yan, A. Kracher, S. T. Hannahs, S. L. Bud'ko, and P. C. Canfield, *Phys. Rev. B* **78**, 214515 (2008).
- [34] E. B. Sonin, *Phys. Rev. B* **48**, 10487 (1993).
- [35] L. M. Paulius, J. A. Fendrich, W.-K. Kwok, A. E. Koshelev, V. M. Vinokur, G. W. Crabtree, and B. G. Glagola, *Phys. Rev. B* **56**, 913 (1997).
- [36] G. Blatter, M. V. Feigel'man, V. B. Geshkenbein, A. I. Larkin, and V. M. Vinokur, *Rev. Mod. Phys.* **66**, 1125 (1994).
- [37] K. Bennemann and J. Ketterson, *The Physics of Superconductors, Vol. I., Conventional and High-Tc Superconductors* (Springer, Berlin-Heidelberg, 2012).
- [38] T. Taen, H. Yagyuda, Y. Nakajima, T. Tamegai, O. Ayala-Valenzuela, L. Civale, B. Maiorov, T. Kambara, and Y. Kanai, *Phys. Rev. B* **89**, 024508 (2014).

- [39] G. Li, W. Z. Hu, J. Dong, Z. Li, P. Zheng, G. F. Chen, J. L. Luo, and N. L. Wang, *Phys. Rev. Lett.* **101**, 107004 (2008).
- [40] M. V. Feigel'man, V. B. Geshkenbein, A. I. Larkin, and V. M. Vinokur, *Phys. Rev. Lett.* **63**, 2303 (1989).
- [41] M. P. Maley, J. O. Willis, H. Lessure, and M. E. McHenry, *Phys. Rev. B* **42**, 2639 (1990).
- [42] T. Taen, Y. Nakajima, T. Tamegai, and H. Kitamura, *Phys. Rev. B* **86**, 094527 (2012).
- [43] K. Itaka, T. Shibauchi, M. Yasugaki, T. Tamegai, and S. Okayasu, *Phys. Rev. Lett.* **86**, 5144 (2001).